Research Square

Preprints are preliminary reports that have not undergone peer review.
They should not be considered conclusive, used to inform clinical practice,
or referenced by the media as validated information.

# Silicification of Living Bone

**Jipin Zhong**

jzhong@sibasebio.com

Silicon Biotechnology (Jiaxing) Co., Ltd

**Article**

**Keywords:** Silicon, Silica, Silicification, Osteogenesis, Living Bone

**Posted Date:** November 13th, 2026

**DOI:** https://doi.org/10.21203/rs.3.rs-11709970/v1

**License:** This work is licensed under a Creative Commons Attribution 4.0 International License.
Read Full License

**Additional Declarations:** No competing interests reported.

# Silicification of Living Bone

Jipin Zhong

*Silicon Biotechnology (Jiaxing) Co., Ltd., 138 Xiuzhou Ave., Future Plaza, Building C Room #802-1, Jiaxing, Zhejiang 314001, China*

Email: jzhong@sibasebio.com

**Abstract**

It has been well recognized that Silicon is an essential trace element in the living body in respect of osteogenesis and connective tissue metabolism of bone. Also, silicon or silica-based biomaterials have proved clinically to be excellent candidates to repair the damaged bone tissue. So far, how silicon interacts with the living tissues and cells to achieve this great osteogenic ability is still unknown. In our world, silicification does occur to form a strong bone structure to some marine organisms with available $SiO_2$ in the ocean and some proteins play important role in that process. Continuing to Search for more osteogenic effects of silicon on the living bone, this work utilized pure silica to fill the sheep femur bone defects to provide a certain available level of silicon or silica. A significant silicification of living bone was indeed observed inside the living bone tissue of the grafted boney defect area in 3 months. Computational modeling using Molecular Orbital Package (MOPAC) indicated the nucleation sites for the formation of silicification could be the same sites for the nucleation of calcification, which are located at the “gap zone” of type I collagen. This preliminary work opens a question if the living bone with mineralization by silicification is as normal as mineralization by calcification, or even better. That will leave to be further evaluated in future works along with continuous searching of the osteogenic ability of silicon in molecular and cellular level and its mechanism.

**Keywords:** Silicon; Silica; Silicification; Osteogenesis; Living Bone

## 1. Introduction

Silicon, an element from any silicates or soluble $SiO_2$, that is silicic acid, in solution, has been long studied and reported as an essential trace element in the living body in respect of osteogenesis and connective tissue metabolism of bone[1,2]. Effects on bone formation were noted for chickens maintained on silicon diets which was reported by Carlisle[3,4], and he showed that minor silicon greatly promoted the bone growth and found the silicon was even present at the mineralization front in growing bone. Also, many studies reported that the dietary Silicon intake would improve the density, regeneration and health of human bone[5,6,7,8,9].

Also in 1970s, silica based Bioglass was invented by Hench as a bioactive material being able to form a chemical bonding with living bone[10]. When Bioglass containing 45% $SiO_2$, presents at physiological environment, or simulated body fluid, a series of surface reactions happen to result in the formation of hydroxy-carbonate-apatite(HCA), a mineral phase of living bone, on its surface[11,12]. The surface binding with collagen of connective tissue, plus the formation of HCA, contribute the strong bonding of Bioglass with living bone[13]. Furthermore, the dissolution products of this silica based Bioglass at physiological environment medium can proliferate bone cell growth[14], active gene expression of osteoblast[15]. These bioactive properties make Bioglass an ideal bone graft material to promote new bone growth fast and repair the bone defects rapidly[16,17]. The bone graft products made from Bioglass have been wildly used clinically in the world over 30 years.

The clinical success of Bioglass[18,19] made a number of researches to incorporate silicon, that is in the form of silica, into some other biomaterials, such as calcium phosphate etc. Some works published that the silicon-incorporated biomaterials demonstrate an enhanced osteogenic ability[20,21,22,23].

However, how silicon interacts with the living tissues and cells to achieve great osteogenic ability in molecular level or cellular level no matter it presents in minor level as an essential trace element or a quite large amount level such as dissolved from Bioglass inside bone still remains to be understood to date.

Mineralization by calcification is critical to health bone. As is well known, calcification is the process by which bone's organic tissues incorporate $Ca^{2+}$ and $PO_4^{3-}$ to form mineralization phase, resulting in high mechanical strength of bone to become structure and support of living body. In comparison, silicification can be thought as a process by which matters incorporate silica, $SiO_2$, by the polymerization of silicic acid, $Si(OH)_4$, from a solution, or in a simply description, a precipitation of $SiO_2$ into matters. Many publications[24,25] called this process as Biosilicification if it occurs in organisms.

In our world, silicification or biosilicification does occur to form a strong bone structure to some marine organisms such as diatoms[26, 27] and sponges[25] etc. Ocean, of cause, contains soluble $SiO_2$ and some proteins inside these marine organisms play major role in the biosolicification process. So far, no reports have been found on the occurrence of silicification in the living body. Here it comes out a question, given a certain level of silicon or silica inside the living bone tissue or boney defect area, does silicification take place along with the usual bone remodeling?

This work has been specifically designed by using an animal defect model to examine if silicon contained materials does really initiate silicification at the grafted area, which could contribute another major factor to promote new bone growth. If this silicification really happens it could give us a new idea of a possible new structure of living bone and may lead to a new guideline for the design of new regeneration biomedical materials. Also, an early study reported[27] that the average failure stress of diatom frustule, a silicified bone structure, would

reach to 1.1 GPa, over 4 times higher than human cortical bone. Hence, the silicification could open a possible route to greatly improve the mechanical strength of living bone.

## 2. Materials and Methods

In this study, in attempt to examine if the silicification could happen inside the living bone, a sheep femur defect model has been used with 2 selected testing materials to fill the defects and empty defects as control. With the consideration to provide high level of silicon, one of the 2 testing materials was pure silica(100% Silica) gel, and another, 45S5 Bioglass. The pure silica gel (G1) was made from sol-gel process (www.angstompore.com, Particle Solutions, LLC, Alachua FL, USA). In details, TEOS was hydrolyzed by D.I. water, followed by condensation to form silica gel and the gel then was dried and heated for stabilization with final average pore size, 75 A°. The silica gel then was ground to particles with particle size range from 200-750 μm.

45S5 Bioglass was invented in 1971 and the composition in weight percent is 45.0% of $SiO_2$, 24.5% of CaO, 24.5% of $Na_2O$ and 6.0% of $P_2O_5$[10]. Many animal defect models study have proved that Bioglass can stimulate new bone formation and growth[11-17]. In this study 90-710μm particles of Bioglass(G2) have been used to fill the defects. This particle size range product is a commercialized bone graft product with trade name NovaBone (www.novabone.com, NovaBone Products, LLC, Alachua FL, USA).

3 plus 1 extra health male mountain sheep with weight from 30-41 Kg have been raised at the testing center for 7 days before implant surgery. Then a 3 months study has been conducted to verify if the silicification occurs. 2 defects would be created at each side of sheep's femur with one defect created in the condyle of femur and another in the Greater Trochanter, as demonstrated in Figure 1. Each animal has one empty defect without any material implanted as control. 5 defects were for G1 material while 4 defects for G2 material and the total defects would be 12 for 3-month testing.

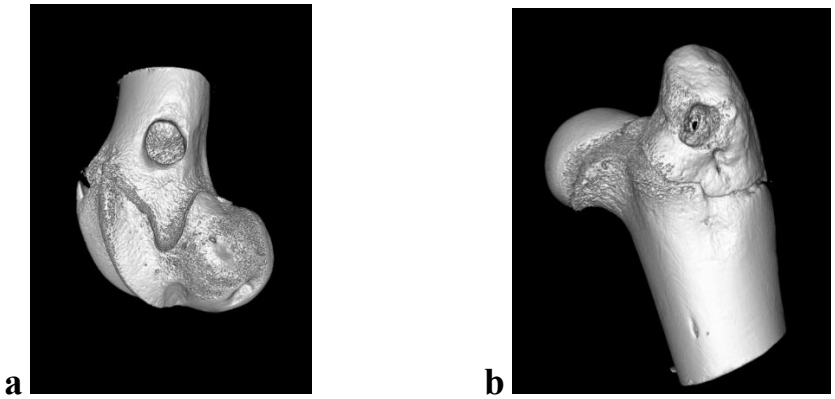



Fig. 1 Macro-CT graphs of defects created at a), the Condyle, and b), the Greater Trochanter, of the sheep femur

During the implant surgery, a standard anesthesia was used and standard skin hair shaving and incising through skin and mussel were conducted to expose the femur bone. A defect with 8mm in diameter and 20mm in depth was created by electronical drills for each defect. Around 1.0-1.1 cc testing materials has been filled to each defect, followed with closure and suturing.

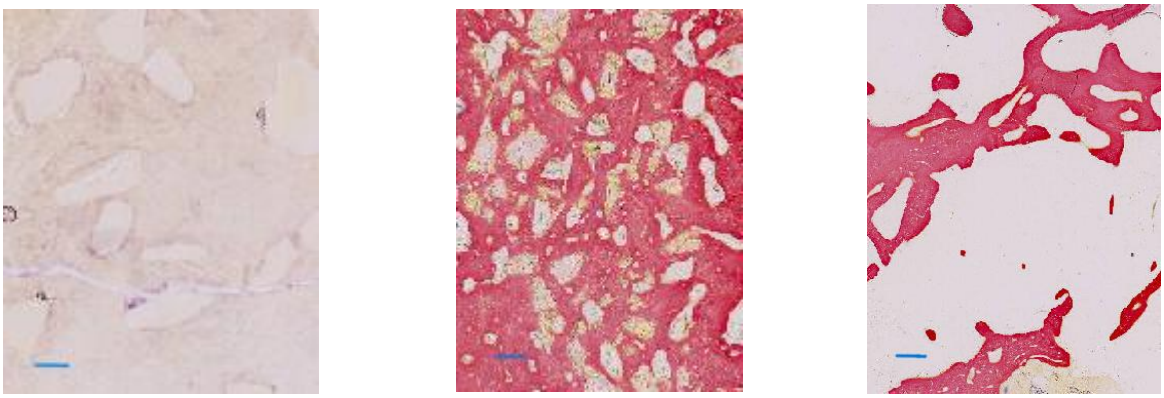
At 3 months, the animals were sacrificed and the all-tested sections were obtained followed by standard procedures to prepare the specimens for the histological analysis and SEM examination. The obtained sections were socked in 10% pH neutral formalin, followed by dehydration. Then, each section was first sliced with one thin piece which was slowly dried in an oven at 37 °C for 10 hours for SEM examination. For the histological analysis, each section tissue continued normal procedures by embedding them with methyl methacrylate (MMA). After embedding procedures each specimen was sliced to 3 pieces with one also for SEM examination, second for HE dyeing for soft tissue pathological evaluations, and third for methylene blue fuchsin dyeing for new bone formation analysis.

**3. Results**

The visual observation of follow up after surgery indicated all animals behaved normal with no any wound infection. Soft tissue pathological analysis also shows no inflammation or

infection inside the grafted defects.

Fig. 2 demonstrates the histological results of the testing, and empty groups in 3 months. No bone formation has been observed for the testing G1 (silica gel) group. For the G2 (Bioglass) group it looks like very normal as always demonstrated in previous works[16]. Empty group showed little bone formation as usual. Since there is no bone could be observed for the G1 group, no statistical analysis has been conducted in this study.



a) Silica Gel b) Bioglass c) Empty

Fig. 2 Histological Examination of a) Silica Gel (Testing G1), b) Bioglass (Testing G2), and c) Empty group implanted for 3 months. Blue Bar in all graphs: 300 μm

Scanning Electron Microscopy (Low-Magnification model Phenom XL, Thermo-Fisher Scientific, Inc.) examination was performed for further analysis to the histological samples from both of testing G1 and G2 groups. For the embedded samples, the preparation was the same as for the histological analysis, just without dyeing. Then, samples would be examined under SEM right after standard Au coating.

The microstructure morphology of G1 sample has been demonstrated in Fig. 3 a) and b), in different magnification. The white parts are grafted particles and the white thin line located at the low left side is the scale bar of this SEM graph. The EDX element analysis of G1 sample qualitatively demonstrated only Si element on particle in b1). The region between particles demonstrated Si element along with some majority of organic components in b2). The

microstructure morphology of G2 sample has been demonstrated in Fig. 4 a) and b), in different magnification with the EDX qualitatively element analysis demonstrating normal Si, Ca, P, and Na elements on Bioglass particle in b1). The region between particles demonstrated Ca, P, and Si also along with some majority of organic components in b2). It can be assumed that the majority of organic components would come from bone organic tissue and embedding material, MMA.

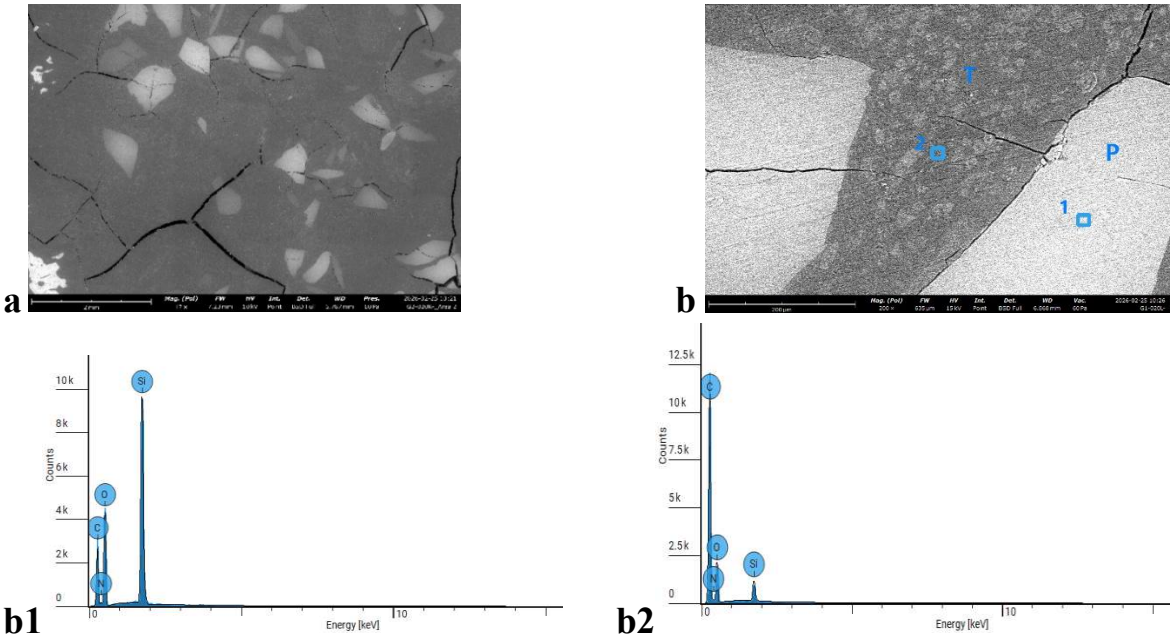
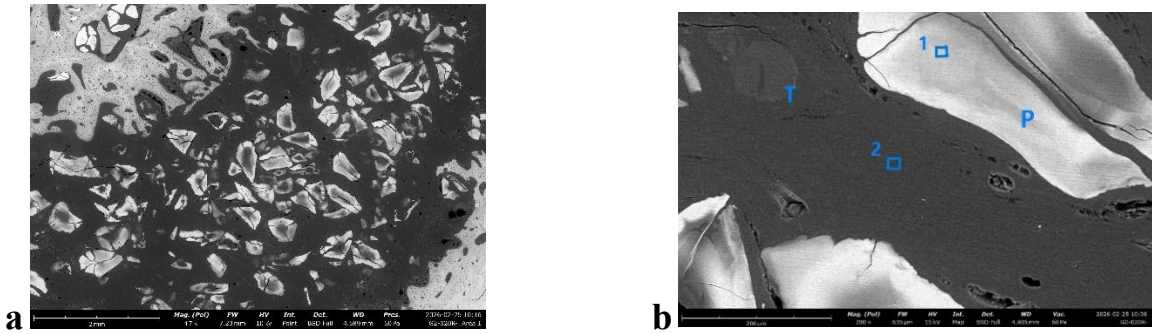



Figure 3 SEM Examination of Histological Microstructure of Silica Gel in Sheep Femoral Condyle Defect in 3 months (Embedded Sample), a) morphology at 17x (Bar in the Graph: 2000 μm); b) morphology at 200x (Bar in the Graph: 200 μm); b1) EDX on particle; b2) EDX on the space between particles. (P – Particles, T – Tissue)



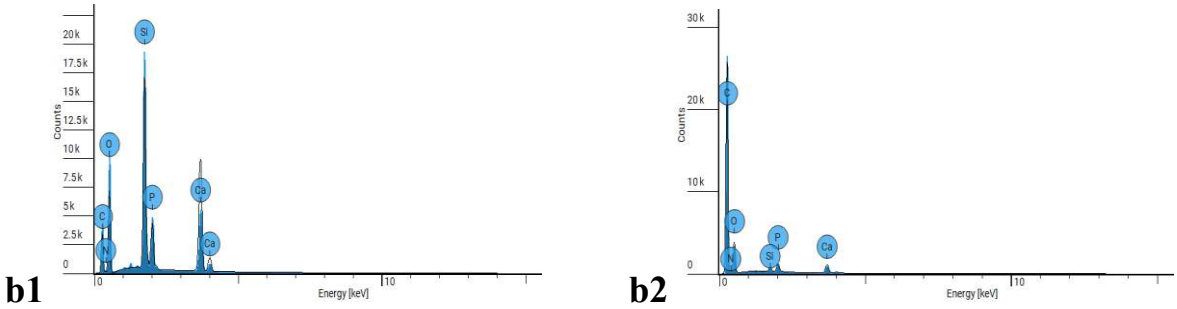
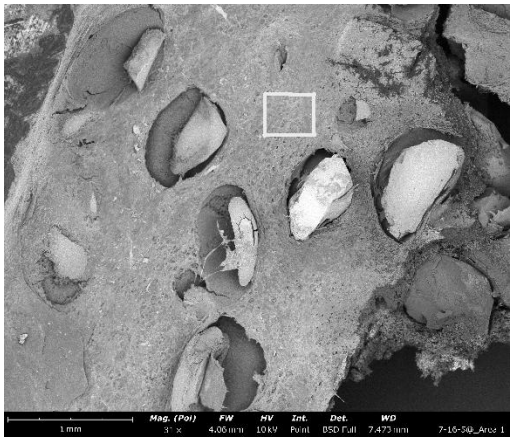


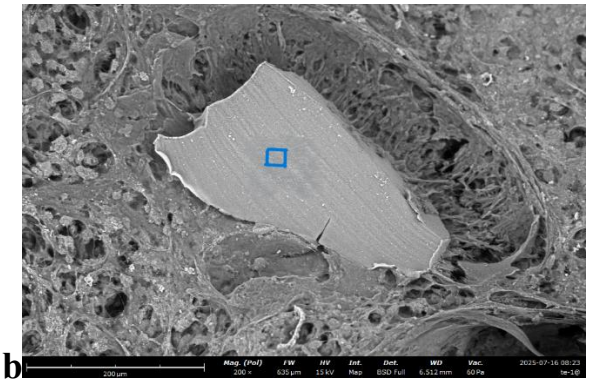

Figure 4 SEM Examination of Histological Microstructure of Bioglass in Sheep Femoral Condyle Defect in 3 months (Embedded Specimen); a) morphology at 17x (Bar in the Graph: 2000 μm); b) morphology at 200x (Bar in the Graph: 200 μm); b1) EDX on particle; b2) EDX on the space between particles. (P – Particles, T – Tissue)

Since the deep level of microstructure could not be examined with the embedded histological samples the prepared unembedded samples were used. As showed in Figs. 5 and 7, low magnification SEM, 40x to high magnification SEM (Phenom Pharos G2, Thermo-Fisher Scientific, Inc.) 100,000x have been used to examine the microstructure of the grafted defect zone. By any magnification, the grafted particles and the extracellular matrix could be clearly identified for both of the testing cases. With the magnification increasing, more microstructure detail could be observed. Although sharp images could not be obtained even at high magnification of 100,000x due to the limited resolution of SEM, nano-sized particles could be identified. Figure 5 a), b), c), d) (low magnification SEM), e), f) (high magnification SEM) demonstrated the microstructure morphology of the unembedded sample from G1 group in an order of increased magnification. EDX element analysis qualitatively demonstrated only Si element on particle in g) and EDX element analysis qualitatively demonstrated Si, Ca and P with dominantly Si element on the space between particles in h). At the high magnification of 100,000x of Fig 5 e) and f), the nano particles can be observed with a round shape estimated ranging 10-20 nm in length and EDX analysis on this zone demonstrated dominantly Si as showed in h).

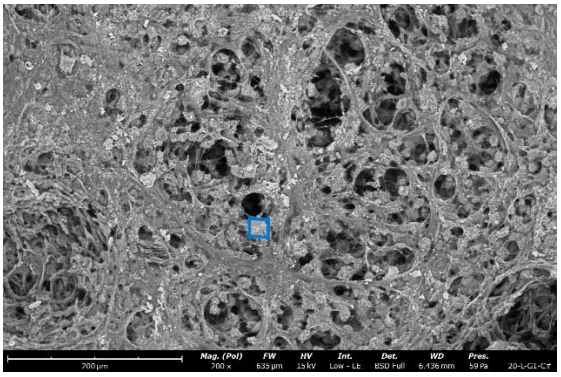
a


1 mm
Mag. (Pol) FW HV Int. Det. WD
4.06 mm 10 kV Point BSD Full 7.473 mm

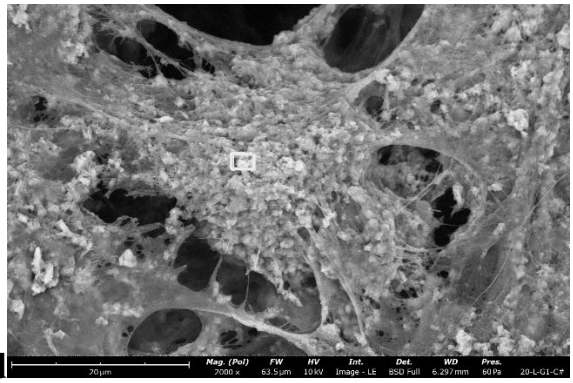
b


200 µm
Mag. (Pol) FW HV Int. Det. WD Vac.
200 x 635 µm 15 kV Map BSD Full 6.512 mm 60 Pa

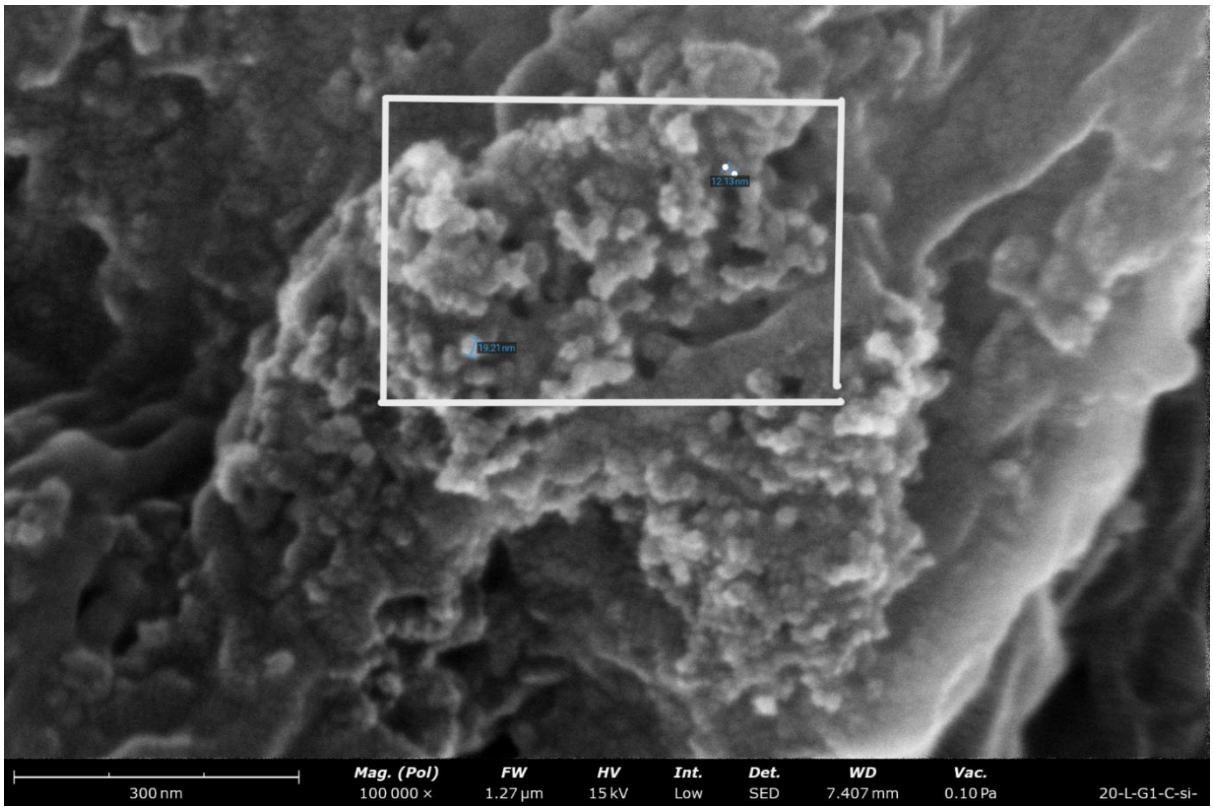
c


200 µm
Mag. (Pol) FW HV Int. Det. WD Pres.
200 x 635 µm 15 kV Low - LE BSD Full 6.436 mm 59 Pa 20-L-G1-C

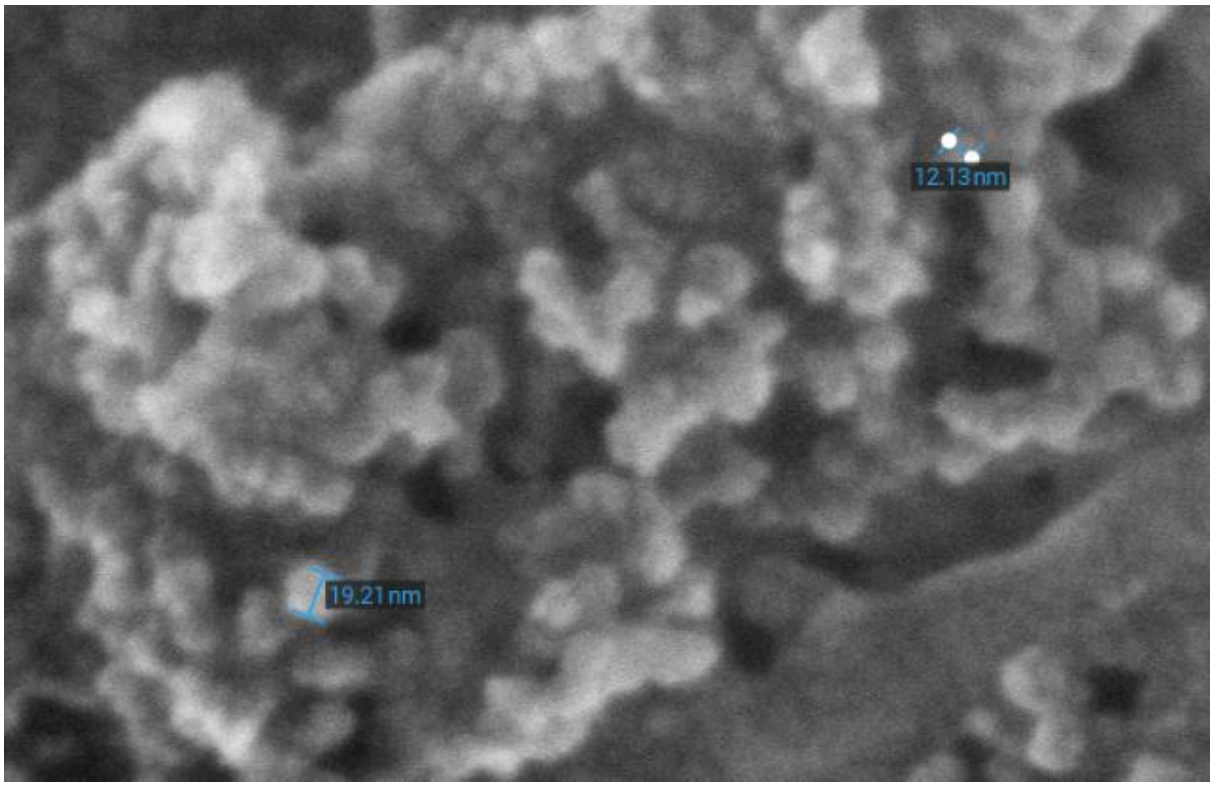
d

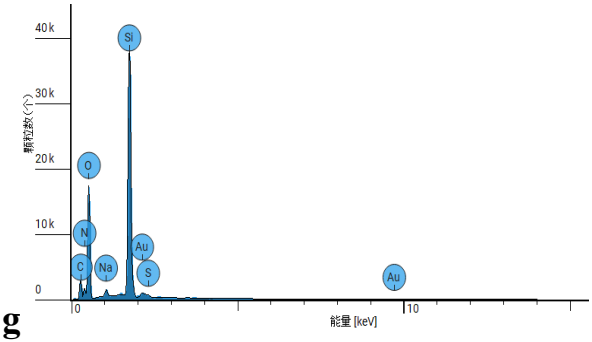

20 µm
Mag. (Pol) FW HV Int. Det. WD Pres.
2000 x 63.5 µm 10 kV Image - LE BSD Full 6.297 mm 60 Pa 20-L-G1-C

e

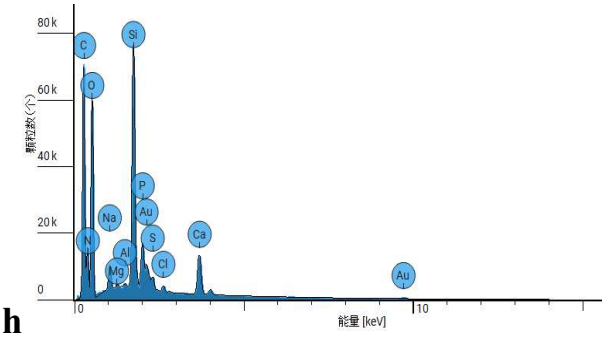

12.18nm
19.21nm
300 nm
Mag. (Pol) FW HV Int. Det. WD Vac.
100 000 x 1.27 µm 15 kV Low SED 7.407 mm 0.10 Pa
20-L-G1-C-si-

**f**




**g**




**h**

Figure 5 SEM Examination of Histological Microstructure of Silica Gel(G1) in Sheep Femoral Condyle Defect in 3 months(Unembedded Sample);

a) By low-magnification 31x (Bar in the Graph: 1000 μm);

b) On a particle 200x (Bar in the Graph: 200 μm);

c) From white square area between particles of a) 200x (Bar in the Graph: 200 μm);

d) From blue square area of c) 2000x (Bar in the Graph: 20 μm);

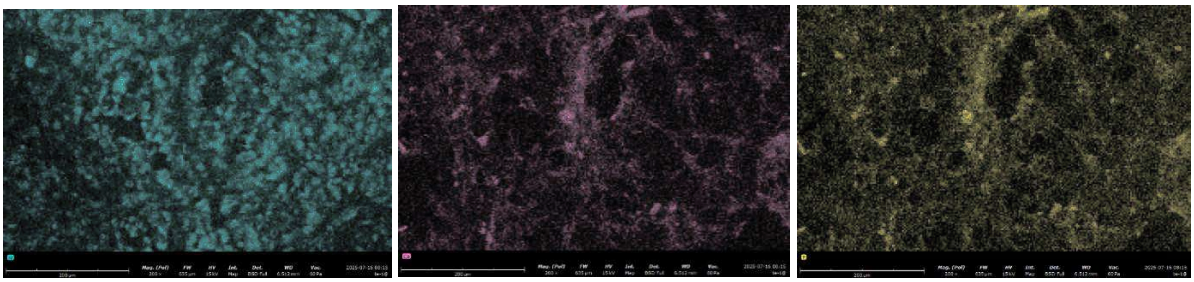
e) By high-magnification of the white square area of d) 100,000x (Bar in the Graph: 300 nm);

f) Enlarge of the white square area of e), the nano-particles estimated ranging from 10-20 nm;

g) EDX on particle of blue square area of b);

h) EDX on the blue square area between particles of c).

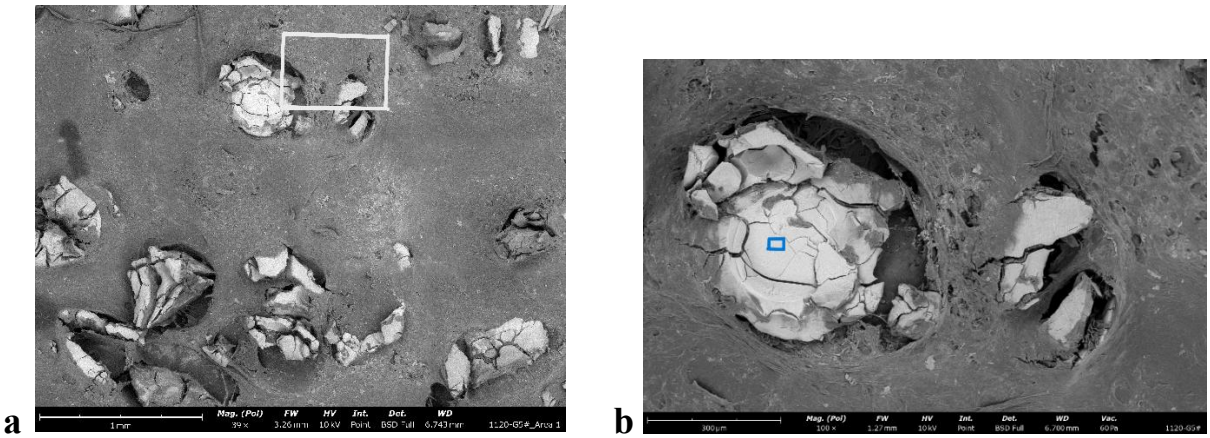
In order to confirm if the Si distributed over the whole area mapping was conducted on the Fig 5 c)(at 200x magnification) of this G1 sample and mapping included Si, Ca and P as showed in Fig 6. Mapping proved that the Si distributed over the whole area.



Si Ca P

Figure 6 Si, Ca and P Mapping on the whole area of Fig 5 c) (at 200x magnification) of the G1 sample (Bar in Graphs: 200 μm).

Figure 7 a), b), c), d) (low magnification SEM) e), f) (high magnification SEM) demonstrated the microstructure morphology of the unembedded sample from Bioglass G2 group in an order of increased magnification. The EDX element analysis qualitatively demonstrated normal Si, Ca, P, and Na elements on Bioglass particle in g). The region between particles demonstrated the mixture of Ca, P, and Si in h), and the nano particles with approximate 16 nm in length can be observed in that region although it is hard to determine the shape of the nano-sized particles. It is possible that both of hydroxyapatite particles and silica particles might be formed.



**a** **b**

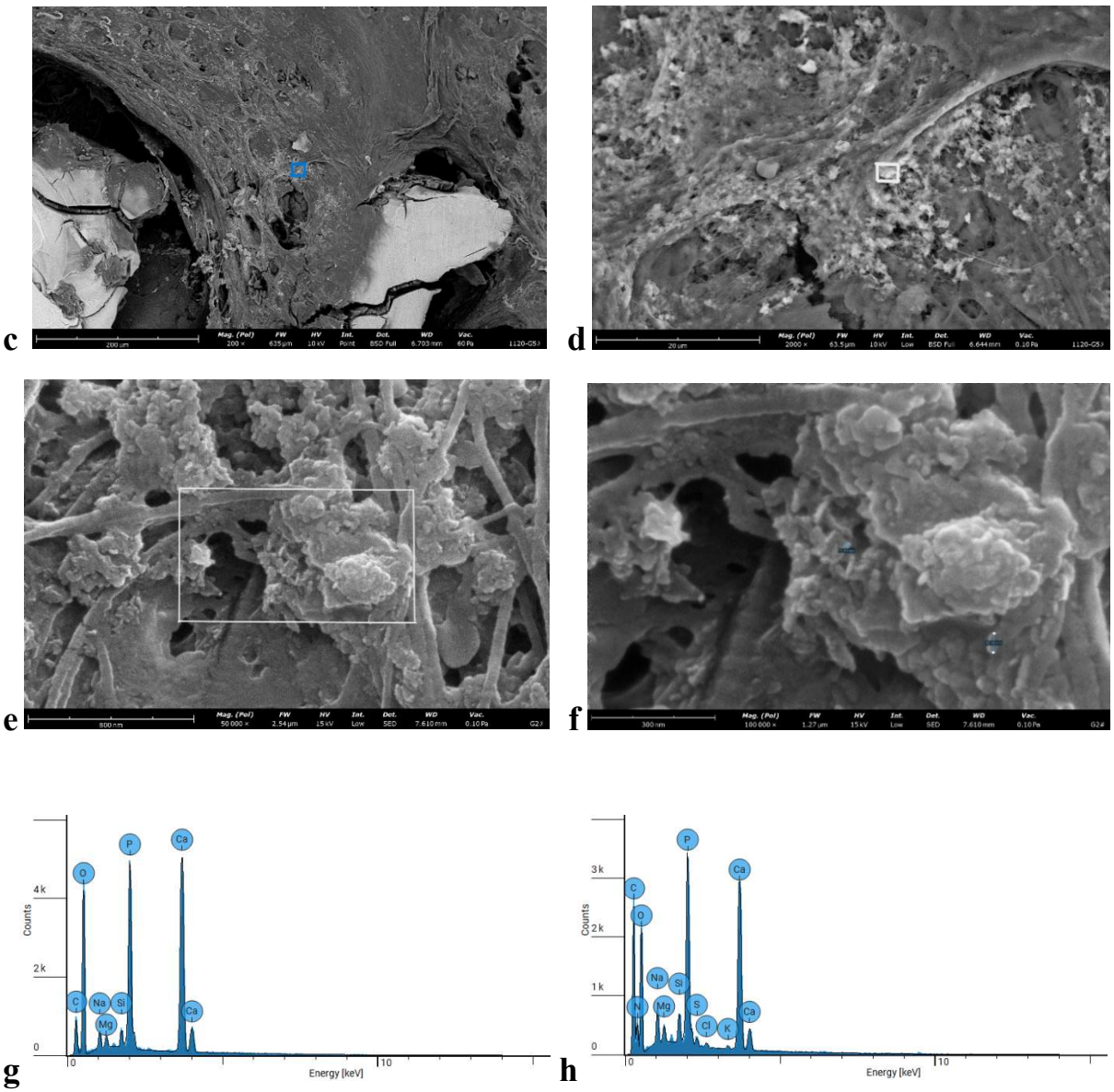



Figure 7 SEM Examination of Histological Microstructure of Bioglass(G2) in Sheep Femoral Condyle Defect in 3 months(Unembedded Sample);

a) By low magnification 39x (Bar in Graphs: 1000 μm);

b) On a particle 100x (Bar in Graphs: 300 μm);

c) From white square area between particles of a) 200x (Bar in Graphs: 200 μm);

d) From blue square area of c) 2000x (Bar in Graphs: 20 μm);

e) By high-magnification of the white square area of d) 50,000x (Bar in Graphs: 800 nm);

f) From white square area of e), 100,000x (Bar in Graphs: 300 nm), the nano-particles around 16 nm;

g) EDX on particle of blue square area of b);

h) EDX on the blue square area between particles of c).

Here it should be explained that for all EDX results above, the relative counts between elements are relevant while the total counts are not because the total counts are influenced by

surface roughness, collecting time and other settings.

## 4. Discussion

### Silicification of Living Bone

After 3 months implantation of the silica gel testing sample into the sheep femur defects significant silicon has been detected on the region between particles as showed in Fig. 5 h) and the nano-sized silica particles have been observed within the extracellular matrix as showed in Fig. 5 e) and f). Therefore, we can call this the silicification of living bone. Silicification has not been found to occur in living body of this world in any published works yet so far. In this animal study, the silicification of the living bone was indeed observed with the polymerized silica particles in round shape and length around 19 nm, similar level as usual mineral hydroxy-apatite particles from the calcification[28,29]. At this physiological condition and body temperature, polymerized silica should be amorphous and the round shape coincides with many published works which used some proteins to obtain the silica particles by silicification processing[26,30,31].

For Bioglass sample, the EDX on its particle in Fig. 7 g) showed Ca and P qualitatively with less Si due to the dissolution of Si and the formation of Hydroxyapatite on the top. On the region between particles in Fig. 7 h), the EDX demonstrated dominantly Ca and P, the normal bone mineral phase components. However, the weak signal of Si was also detected on that region. It can be assumed that silicon based Bioglass could also make the silicification happen although it might be a small portion compared with the total mineral phase of the new bone. When we go back to review the histological graph of Fig. 2 a) of silica gel particles grafted defect in the above Results section, grafted particles can be observed but no new bone tissue can be observed. Now it can be assumed that it is a silicified bone, instead of calcified bone and current dye and optical microscopy method is designed to observe mineralization by calcification, not silicification.

**Polymerization of Silica**

Bone provides structure and support for the living body, possessing mechanical strength resulting from the mineralization of living bone by the calcification processing. It has been well accepted that the calcification derived mineralization is directly related to some physical and chemical reactions in the extracellular matrix (ECM)[32], and the level of the ionic calcium and phosphate groups are two critical determinants for bone mineralization[33]. Also, as a well-recognized mechanism, there are some side-chains with negatively charged carboxyl groups ($COO^{-1}$) on the collagen, especially at the "Gap Zone" (or "Hole Zone"), which serve as nucleation sites for the mineralization of living bone [34,35,36]. These side chain groups are mainly from Aspartate and Glutamate etc., the negatively charged amino acids which collagens contain.

In this *in vivo* study, the silicification derived mineralization has been found for the living bone, and there is a good reason to believe this process can be also related to physical and chemical reactions in the same manner as calcification does[32]. Once silica gel particles have been implanted into the defect, the dissolution would generate soluble silica, or silicic acid in the surrounding area. Solid silica possesses low solubility in aqueous solution at room temperature and the polymerization of soluble silica would not occur in the equilibrium solution, but occur in two conditions: supersaturated silica or the existence of nucleation sites[37]. In the experiment condition of this study, the soluble silica from the silica gel-based graft particles dissolved into the defect area reaching thermodynamic equilibrium and the supersaturation of silica in the defect area would not exist. Therefore, the occurrence of soluble silica polymerization in this experiment should result from the external factor, that is, the existence of nucleation sites.

Although silicification of bone has not been reported to occur in living body to this day, however it occurs on some of marine organisms such as diatom and sponge etc. as mentioned

above[25, 26]. Many studies have been conducted on the silicification or biosilicification of diatom and sponge in attempt to understand the mechanism behind the process. In an early study in 1973, Hecky reported protein could serve as a template for the Si-deposition in the diatom walls[38]. Later, Perry published that the protein, silaffin would serve as a template and silicatein as enzyme for the silicification processing[39]. Therefore, it can be said the silicification is protein mediated process. And these proteins serve as the external factors creating nucleation sites for the polymerization of silica, that is, silicification. So far, the important findings to explain the process of the biosilicification in diatom could be the published works from computational modeling. Lobel and Hench[40, 41] used semi-empirical Molecular Orbital model (MOPAC) to calculate the soluble silica-proteins reaction at the interface. They adopted the β-sheet configuration from the protein-rich template to investigate the polymerization of soluble silica onto the β-sheet. The modeling resulted in the formation of 4-member ring silica stable structure, and the overall reaction was downhill in the heat of formation, indicating an autopolymerization process. Thus, that work has offered evidence for the biosilicification process, a low activation barrier reaction pathway for the nucleation and growth of silica in the diatom.

**Molecular Orbital Computational Modeling of Silica Polymerization**

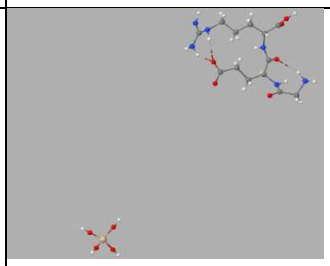
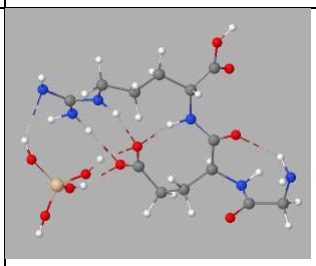
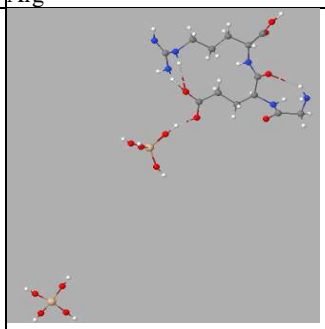
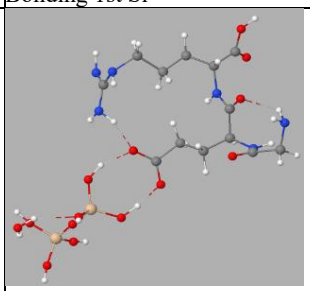
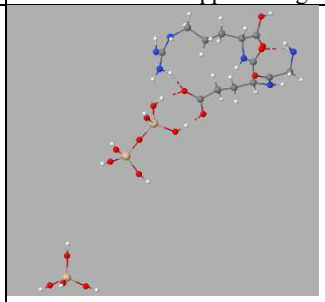
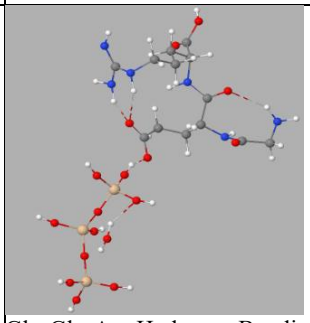
In this study, under the direct guidance of Professor James J. P. Stewart, the developer of Molecular Orbital Computational Modeling Package (MOPAC), a semiempirical computational program[42,43], I have used the MOPAC2016 (https://openmopac.com) with PM6-D3H4 method[44] to model and calculate the thermodynamic process of the Silicification. I also used the same nucleation sites of the calcification in the collagen “Gap Zone” with negatively charged carboxyl groups[34,35,36] as the reaction site between the soluble silicas and the negatively charged carboxyl group. As a common knowledge, Collagen structure consists

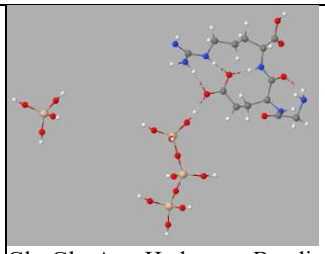
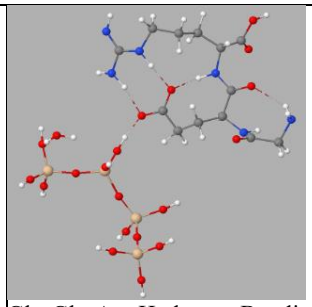
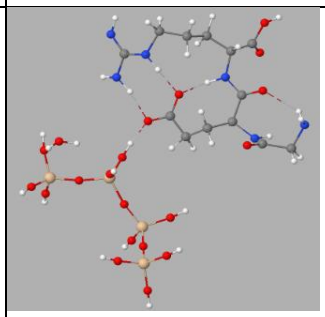
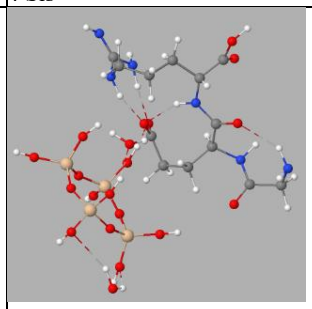
of 3 repeated amino acids as Glycine(Gly) always leading this 3 repeated amino acids(called tripeptides)[45]. In this modeling, Glycine-Glutamate-Arginine(Gly-Glu-Arg) tripeptide, which exists in the nature type I collagen[45], has been chosen as the base to simulate the case with negatively charged carboxyl group from Glutamate. The model designed here is as the 4 silicic acids approaching the Gly-Glu-Arg to eventually form 4 Si-member ring, and the reactions were modeled by MOPAC PM6-D3H4 calculation. The calculation results are listed in the Table I.

When the 1st silicic acid approached the Gly-Glu-Arg, a strong hydrogen bonding occurred with difference of Heat of Formation $\Delta H_f$ reached to -39.81 Kcal/mol, much greater than usual hydrogen bonding strength from -4 to -20 Kcal/mol [46,47]. McCutchin etc. also reported that hydrogen bonding between silicic acid and amino acids or polysaccharides promoted the biosilicification[48]. This hydrogen bonding can occur without much energy barrier to overcome. This strong hydrogen bonding likely hindered the further covalent bonding happen to form Si-O-C, which was indicated by MOPAC modeling. Once the 1st silicic acid has been bonded with this tripeptide, then other silicic acid will approach to form silica chain and ring by polycondensation or polymerization. The modeling has 5 steps of reactions as demonstrated in Table I, to eventually form 4 Si-member ring. Therefore, this negatively charged side chain of Glu from collagen serves as nucleation site for the silica. Table I demonstrates the entire process of the formation of 4 Si-member ring with hydrogen bonding to Gly-Glu-Arg and all of the thermodynamic data for the reactions. The entire reaction is downhill thermodynamically indicating the formation of silica ring is stable. During the modeling the transition highest energy state was calculated by Saddle process, which was the barrier of each reaction. Then, the activation energy of each reaction was calculated by the difference between the highest energy and the reactant energy state.

In the real bone tissue environment, it would be rich with negatively charged side chain groups in the “Gap Zone” of collagen. The silicic acids would be accumulated there through hydrogen bonding to the negatively charged group and eventually form the silica networks with 3, 4, 5 and 6 member rings, the silica polymerization, resulting in the formation of amorphous silica, that is, silicification.

Table I Molecule Structure and Thermodynamic Data for the Reaction between Silicic Acid and Negatively Charged Carboxyl Group of Gly-Glu-Arg Side Chain to Form 4 Si-Member Ring
(In the molecule structure, -Si, -C, -N, -O, -H)

| Step # | Reactants | | Product | | Difference of $H_f$ , $\Delta H_f$=$H_f$(P)-$H_f$(R) (Kcal/Mol) | Saddle Point(Kcal/Mol) | Activation Energy(Ea, Kcal/Mol) |
|---|---|---|---|---|---|---|---|
| | Molecule Processing | Heat Formation ($H_f$, Kcal/Mol) | Molecule Processing | Heat Formation ($H_f$, Kcal/Mol) | | | |
| 1 |  The 1st Si Approaching Gly-Glu-Arg | -613.03 |  Gly-Glu-Arg Hydrogen Bonding 1st Si | -652.84 | -39.81 | - | N/A |
| 2 |  Gly-Glu-Arg Hydrogen Bonding 1st Si with 2nd Si Approaching | -936.49 |  Gly-Glu-Arg Hydrogen Bonding 2 Sis | -944.02 | -7.53 | -904.36 | 32.13 |
| 3 |  Gly-Glu-Arg Hydrogen Bonding 2 Sis with the 3rd Si Approaching | -1186.66 |  Gly-Glu-Arg Hydrogen Bonding 3 Sis | -1200.33 | -13.67 | -1159.95 | 26.71 |

| | | | | | | | |
|---|---|---|---|---|---|---|---|
| 4 |  Gly-Glu-Arg Hydrogen Bonding 3 Sis with 4th Si Approaching | -1450.77 |  Gly-Glu-Arg Hydrogen Bonding 4 Sis | -1454.06 | -3.29 | -1419.77 | 31.00 |
| 5 |  Gly-Glu-Arg Hydrogen Bonding 4 Sis | -1454.06 |  Gly-Glu-Arg Hydrogen Binding 4 Si-Member Ring | -1480.63 | -26.57 | -1418.00 | 36.06 |

## 5. Conclusion

In this study, grafted with pure silica gel particles to the sheep femur defects, significant silicification was indeed observed in the grafted defect area. Theoretically, Molecular Orbital Computational Modeling proved that the negatively charged side groups from type I collagen would serve as nucleation site for the polymerization of silica, resulting in the silicification of living bone.

This discovery could provide a new idea for the new biomedical materials selection and new medical products designing. Meanwhile, this preliminary work opens a question if the living bone with mineralization by silicification is as normal as mineralization by calcification, or even better. The future works need to continue to find the answer along with continuous searching of the osteogenic ability of silicon in molecular and cellular level.

## 6. References

1 Carlisle, E.M. Silicon: A Possible Factor in Calcification. *Science* **167**, 279-80 (1970)

2 Schwarze, K., Milne, D.B. Growth-Promoting Effects of Silicon in Rats. *Nature* **239**, 333-334 (1972)

3 Carlisle, E.M. Silicon: An Essential Element for the Chick. *Science* **178**, 619-621 (1972)

4 Carlisle, E.M. Silicon as an Essential Element. *Federation Proceedings* **33** (6), 1758-1766 (1974)

5 Nielsen, F.H. Update on the Possible Nutritional Importance of Silicon. *J. Trace Elem. Med. Biol.* **28**, 379-382 (2014)

6 Jugdaohsingh, R., et al. Dietary Silicon Intake is Positively Associated with Bone Mineral Density in Men and Premenopausal Women of the Framingham Offspring Cohort. *J. Bone Min. Res.* **19**, 297-307 (2004)

7 Jugdaohsingh, R. et al. Dietary Silicon Intake and Absorption. *Am J Clin Nutr.* **75**, 887-893 (2002)

8 Beck Jr, G.R. et al. Bioactive Silica Based Nanoparticles Stimulate Bone Forming Osteoblasts, Suppress Bone Esorbing Osteoclasts, and Enhance Bone Mineral Density in Vivo. *Nanomedicine* **8**(6), 793-803 (2012)

9 Kim, E.J., Bu, S.Y., Sung, M.K., Choi, M.K. Effects of Silicon on Osteoblast Activity and Bone Mineralization of MC3T3-E1 Cells. *Biol. Trace Elem. Res.* **152**(1), 105-112 (2013)

10 Hench, L.L. et al. Bonding Mechanism of the Interface of Ceramic Prosthetic Materials. *J. Bioed. Maters. Res.* **2**(1), 117-141 (1972)

11 Hench, L.L. Bioceramics: From Concept to Clinic. *J. Am. Ceram. Soc.* **74**, 1487-1510 (1991)

12 Hench, L.L., West, J.K. Biological Application of Bioactive Glasses. *Life Chem. Report* **13**, 187-241 (1996)

13 Zhong, J.P., LaTorre, G.P., Hench, L.L. The Kinetics of Bioactive Ceramics Part VII: Binding of Collagen to Hydroxyapatite and Bioactive Glass. *Bioceramics* **7**, 61-66 (1994)

14 Xynos, I.D. et al. Ionic Products of Bioactive Glass Dissolution Increase Proliferation of Human Osteoblasts and Induce Insulin-like Growth Factor II mRNA Expression and Protein Synthesis. *Biochem. Biophys. Res. Commun.* **276**, 461-465 (2000)

15 Xynos, I.D. et al. Gene-Expression Profiling of Human Osteoblasts Following Treatment with the Ionic Products of Bioglass 45S5 Dissolution. *J. Biomed. Mater. Res.* **55**, 151-157 (2000)

16 Wang, Z. et al. Evaluation of an Osteostimulative Putty in the Sheep Spine. *J. Mater. Sci: Mater. Med.* **22**, 185-191 (2010)

17 Okay, E. et al. The Biocompatibility of a New type of 45S5 Bioactive Graft in a Sheep Model: A Pilot Study. *Cureus* **15**(7), doi: 10.7759/cureus.41521 (2023)

18 Zamet, J.S. et al. Particulate Bioglass as a Grafting Material in the Treatment of Periodontal Intrabony Defects. *J. Clin. Period.* **24**, 410-418 (1997)

19 Ilharreborde, B. et al. Bioactive Glass as a Bone Substitute for Spinal Fusion in Adolescent Idiopathic Scoliosis: A Comparative Study with Iliac Crest Autograft. *J. Pediatr. Orthop.* **28**, 347-351 (2008)

20 Götz, W., Tobiasch, E., Witzleben, S., and Schulze, M. Effects of Silicon Compounds on Biomineralization, Osteogenesis, and Hard Tissue Formation. *Pharmaceutics* **11**(3), 117-144 (2019)

21 Pietak, A.M., Reid, J.W., Stott, M.J., Sayer, M. Silicon Substitution in the Calcium Phosphate Bioceramics. *Biomaterials* **28**(28), 4023-4032 (2007)

22 Hing, K.A., Revell, P.A., Smith, N., Buckland, T. Effect of Silicon Level on Rate, Quality and Progression of Bone Healing within Silicate-Substituted Porous Hydroxyapatite Scaffolds. *Biomaterials* **27**, 5014-5026 (2006)

23 Shao, Y.K. et al. Silicocarnotite: Novel Silicate Bioceramic with Osteogenic Property for Repairing Rat Cranial Critical-Sized Bone Defects. *Frontiers in Materials* **9**, doi: 10.3389/fmats.2022.919029 (2022)

24 Ikeda, T. Bacterial Biosilicification: A New Insight into the Global Silicon Cycle. *Bioscience, Biotechnology, and Biochemistry*, **85** (6), 1324-1331 (2021)

25 Otzen, D. The Role of Proteins in Biosilicification. *Scientifica* http://dx.doi.org/10.6064/2012/867562 (2012)

26 Poulsen, N., Kröger, N. Silica Morphogenesis by Alternative Processing of Silaffins in the Diatom *Thalassiosira pseudonana*. *J. Biolog. Chem.* **279** (41), 42993-42999 (2004)

27 Aitken, Z.H. et al. Microstructure provides insights into evolutionary design and resilience of Coscinodiscus sp. Frustule. *PANS* **113**, 2017-2022 (2016)

28 Wang, B., Zhang, Z.Q., Pan, H.B. Bone Apatite Nanocrystal: Crystalline Structure, Chemical Composition, and Architecture. *Biomimetics* **8**(1), 90 (2023)

29 Shah, F.A. Revisiting the Physical and Chemical Nature of the Mineral Component of Bone. *Acta Biomaterialia* **196**, 1-16 (2025)

30 Patwardhan, S.V., Clarson, S.J. Silicification and Biosilicification: Part 4. Effect of Tempate Size on the Formation of Silica. *J. Inorg. And Org. Poly.* **12**, 109-116 (2002)

31 Kröger, N., Deutzmann, R., Sumper, M. Polycationic Peptides from Diatom Biosilica That Direct Silica Nanosphere Formation. *Science* **286** (5), 1129-1132 (1999)

32 van der Meijden, R.H.M., et al. A 3D Cell-Free Bone Model Shows Collagen Mineralization is Driven and Controlled by the Matrix. *Adv. Funct. Mater.* **33**, (https://doi.org/10.1002/adfm.202212339) (2023)

33 Murshed, M. Mechanism of Bone Mineralization. *Cold Spring Harb Perspect. Med*. **8**, doi: 10.1101/cshperspect.a031229 (2018)

34 Xu, Z. J. et al. Molecular Mechanisms for Intrafibrillar Collagen Mineralization in Skeletal Tissues. *Biomaterials* **39**, 59-66 (2015)

35 Indurkar, A. et al. Role of Carboxylic Organic Molecules in Interfibrillar Collagen Mineralization. *Front. Bioeng. Biotechnol*. (https://doi 10.3389/fbioe.2023.1150037) (2023)

36 William J.L., Frederick, H.S. Mineral Deposition in the Extracellular Matrices of Vertebrate Tissues: Identification of Possible Apatite Nucleation Sites on Type I Collagen. *Cells Tissues Organs* **189**, 20-24 (2009)

37 Scott, S. et al. Silica Polymerization and Nanocolloid Nucleation and Growth Kinetics in Aqueous Solutions. *Geochimica et Cosmochimica Acta* **371**, 78-94 (2024)

38 Hecky, R.E. et al. The Amino Acid and Sugar Composition of Diatom Cell-Walls. *Marine Biology* **19**, 323-331 (1973)

39 Perry, C.C., Keeeling-Tucker, T. Biosilicification: The Role of the Organic Matrix in Structure Control. *J. Biol. Inorg. Chem.* **5**, 537-550 (2000)

40 Lobel, K.D., West, J.K., Hench, L.L. Computational Model for Protein-Mediated Biomineralization of the Diatom Frustule. *Marine Biology* **126**, 353-360 (1996)

41 Lobel, K.D., West, J.K., Hench, L.L. Molecular Orbital Model of the Diatom Frustule: Potential for Biomimetics. *J. Mat Sci Lett* **15**, 648-650 (1996)

42 Stewart, J., MOPAC: A Semiempirical Molecular Orbital Program. *J. Computer-Aided Molecular Design* **4**, 1-105 (1990)

43 Moussa J., Steward J. MOPAC: An Open-Source Semiempirical Molecular Orbital Program. *J. of Open-Source Software* **11**(119), 1-4 (2026)

44 Řezáč, J., Hobza, P. Advanced Corrections of Hydrogen Bonding and Dispersion for Semiempirical Quantum Mechanical Methods. *J. Chem. Theory Comput.* **8**, 141-151 (2012)

45 Dölz, R., Heidemann, E. Influence of Different Tripeptides on the Stability of the Collagen Triple Helix. I. Analysis of the Collagen Sequence and Identification of Typical Tripeptides. *Biopolymers* **25**, 1069-1080 (1986)

46 Perrin, C.L., Nielson, J.B. "Strong" Hydrogen Bonds in Chemistry and Biology. *Annual Review of Physical Chemistry* **48**, 511-544 (1997)

47 Graham, J.D. et al. Strong, Low-Barrier Hydrogen Bonds May Be Available to Enzymes. *Biochemistry* **53**(2), 344-349 (2014)

48 McCutchin, C.A. et al. Silica - Biomacromolecule Interactions: Toward a Mechanistic Understanding of Silicification. *Biomacromolecules* **26**, 43-84 (2025)

## Methods

**Animal Surgery**

All animal research was performed in accordance with the guidelines for care and use of animals including SSMT-PAS-007 -《Use and management of the experimental animals in preclinical animal study》, SSMT-SEC-001 -《Management of animal facilities and cleanrooms》, SSMT-SEC-003 -《Laboratory animal feeding and management 》made by **Jiangsu Kebio Medical Technology Group Co., Ltd**. with animal study permission # SYXK(Su) 2021-0012. All procedures in this study were approved by the Institutional Animal Care and Use Committee, Jiangsu Kebio Medical Technology Group Co., Ltd. with doc # IACUC25-0062. Sheep were raised in the facility at 16–28 °C and 30–70% humidity.

**Preparation prior to Surgery**

3 plus 1 extra health male mountain sheep with weight from 30-41 Kg were raised at the testing center for 7 days and passed quarantine tests and meet the test requirements before implant surgery. The sheep were fasted for 24 hours with no water for 4 hours before surgery and were anesthesia induced by intramuscular injection of Xylazine Hydrochloride. And then, endotracheal intubation was used for continuous anesthesia respiration to maintain anesthesia state during the surgery.

**Surgery**

Implantation to femur condyle: Sheep was lied on one side and subcutaneous tissue on distal femur was separated to expose the femur condyle and 8 x 20 mm defect was created as demonstrated in Fig. 1 a. The testing or control materials was filled into the defect to full. And then, the defect was closed and the wound was sutured in a stand procedure.

Implantation to femur Great Trochanter: The same implant surgery was conducted to the Great Trochanter location as demonstrated in Fig. 1 b

**Postoperative care and follow-up**

After recovery of consciousness, the animals were moved to the facility and housed in single cage separately. The intramuscular injections with Ceftiofur Sodium were given for the first 7 days to prevent postoperative infection, and also intramuscular injection with Tolfenamic Acid for the first 3 days postoperatively to reduce pain. During the period of care time, restricted diets were administered. The sheep were housed and raised for 13 weeks postoperatively and no restrictions on animal activity during the period of care time.

General observations were conducted daily before and after surgery with recording. The surgical and implant sites were observed with recoding after surgery to inspect inflammation, suppuration, bleeding, chronic nonhealing wound, sample prolapse, tissue necrosis and gangrene.

**Animal Euthanasia**

At 13 weeks, animals underwent euthanasia in terms of the Standard Operation Procedures with Doc #SSMT-PAS-009《Euthanasia, gross anatomy, ex vivo tissue reuse, and cadaver disposal of experimental animals in preclinical animal study》made by Jiangsu Kebio.

**Specimens Preparation**

**a. Specimens for Histological Analysis**

After euthanasia, the bone sections containing the implanted area of each animal were obtained and the specimens then were soaked in 10% neutral Formalin solution for the fixation for 7 days, followed by dehydration for 12 days. As an imbedding process after dehydration, the specimens were infiltrated

with gradually concentrated MMA(Methyl Methacrylate) solutions for 14 days, followed by final light-curing to harden the specimens.

Each imbedded specimen was sliced along cross-section with diamond saw to 3 thin pieces containing the defect area, and the thin piece specimens then were polished on the surface. One thin specimen was used by HE(Hematoxylin and Eosin) dye for soft tissue evaluation. Another thin specimen was dyed with Methylene Blue Acid Fuchsin for bone formation evaluation. The third thin specimen was just used for SEM examination without any dyeing.

**b. Specimens for SEM Examination**

For better SEM examination, bone section without imbedding from each group was sliced to obtain a thin piece of specimen with fresh tissue. The thin specimens were dried in an oven at 37 °C for 10 hours.

**SEM Examination**

The SEM examination was conducted at Shanghai Testing Center of Phenom China (Shanghai) Scientific Instruments Co., Ltd. (Room 705, T5, 88 Shenbin Road, Shanghai, China), which is owned by Thermo-Fisher Scientific, Inc. All specimens were coated by Au to improve the electronical conductivity as a standard procedure. A clear low-magnification analysis used a Low-Magnification SEM with model, Phenom XL, and a high-resolution analysis used a High-Magnification (Field Emission) SEM with model, Phenom Pharos G2.

**Molecular Orbital Computational Modeling**

The interaction between soluble silica, represented by silicic acid, and a side group of type I collagen was modeled using MOPAC 2016 with the PM6-D3H4 method. The molecular structures and reaction steps were constructed using the Avogadro molecular editor. MOPAC, developed by Professor James J. P. Stewart, together with the PM6-D3H4 method developed and evaluated by Řezáč and Hobza, provides a computational framework that accounts for hydrogen-bonding interactions and London dispersion forces. Geometry optimization of the molecular species involved in each reaction step was used to determine the corresponding changes in heat of formation. Transition-state calculations were also performed to identify the saddle point and thereby estimate the activation energy for the reaction. Because the molecular-orbital calculations are focused on the specific molecular fragments directly involved in the interaction, it is not necessary to include the complete collagen molecule or entire collagen helix in the construction and optimization of each reaction step.

During the modeling process, Avogadro was first used to construct the molecule reaction, and generate an input file. Then, the input file would be used to run the MOPAC 2016 program with PM6-D3H4 as method resulting in an output file containing the heat of formation and a HTML file with final molecule structure.

In this work, side group, of type I collagen bonding to 4 Si member ring has been modeled with 5 reaction steps involved. During the modeling when the first silicic acid approached to the negatively charged side group of type I collagen less than 5Å the strong hydrogen bonding formed, which is the most important reaction as a nucleation site. The outcomes from this modeling calculation are the heat of formation change, that are, before and after reaction and the activation energy for each step reaction to form a 4 Si member ring.

## Statements and Declarations


### Acknowledgement

The author greatly appreciates Professor James J. P. Stewart for his education and direct guidance for the Molecular Orbital Computational Modeling during this study and data collection and verification for the preparation of this manuscript.

### Funding

The author declares that no funds, grants, or other support was received for this study.


### Author Contribution

Jipin Zhong wrote the manuscript and read and approved the final manuscript.

### Competing Interests

The author has no relevant financial or non-financial interests to disclose.

#### Ethical Approval

By Institutional Animal Care and Use Committee, Jiangsu Kebio Medical Technology Group Co., Ltd., Doc # IACUC25-0062.

### Data and Software Availability

All of the data from animal study and MOPAC modeling are available upon request.